Numerical Modeling of ISS Thruster Plume Induced Contamination Environment

A. A. Alexeenko[¶], D.C. Wadsworth[¶], S.F. Gimelshein[§], and A. D. Ketsdever[†]

[¶] *ERC, Inc., Edwards AF Base, CA 93524*

[§] *University of Southern California, Los Angeles, CA 90089*

[†] *Propulsion Directorate, AF Research Laboratory, Edwards AF Base, CA 93524*

1   Introduction

Assessment of thruster induced contamination of critical surfaces is the important and necessary stage of International Space Station (ISS) component design. Plume contamination models aimed at the prediction of the spatial distribution of contaminant mass fluxes have been developed in the recent years for various ISS thrusters based on vacuum chamber and space flight experiments and empirical correlations [1, 2]. Relatively scarce space flight contamination data have been gathered to date and are mostly limited to the measurements of thruster plume centerline contaminant fluxes. It is necessary, however, to have detailed knowledge of the contaminant deposition as a function of the angle from the plume centerline, especially, in the plume backflow region. The realization of this fact has motivated new flight experiments which are being planned for a future Space Shuttle mission [3].

Numerical modeling of thruster efflux transport and deposition on spacecraft surfaces can help to verify and improve the empirical plume contamination models. Strong rarefaction of plume backflow and atmosphere around ISS requires a molecular, kinetic approach to be used. The direct simulation Monte Carlo (DSMC) method based on the kinetic theory of gases has been successfully applied in the last decade for prediction of the molecular contaminant fluxes for various spacecraft plumes [4, 5] and outgassing sources [6]. A continuum approach for the internal part of the nozzle and the DSMC method for plume nearfield was used in [7], where propellant droplets where modeled using a Lagrangian particle tracking. The importance of droplets originated at the cooling film in the region of the nozzle lip was also emphasized in [7].

The principal goal of the present work is to examine both particulate and molecular contaminant transport for a 130 N bipropellant thruster, a typical small thruster used on ISS, and analyze their relative importance near the plume axis as well as in the back flow region in order to provide useful data for comparison with ground-based and space flight

Report Documentation Page

1. REPORT DATE **21 JUL 2004**	2. REPORT TYPE	3. DATES COVERED **-**

4. TITLE AND SUBTITLE	5a. CONTRACT NUMBER
Numerical Modeling of ISS Thruster Plume Induced Contamination Environment	**F04611-99-C-0025**
	5b. GRANT NUMBER
	5c. PROGRAM ELEMENT NUMBER

6. AUTHOR(S)	5d. PROJECT NUMBER
A Alexeenko; D Wadsworth; S Gimelshein; A Ketsdever	
	5e. TASK NUMBER **2308**
	5f. WORK UNIT NUMBER **M19B**

7. PERFORMING ORGANIZATION NAME(S) AND ADDRESS(ES) **ERC Incorporated,AFRL/PRS,10 E. Saturn Blvd.,Edwards AFB,CA,93524**	8. PERFORMING ORGANIZATION REPORT NUMBER

9. SPONSORING/MONITORING AGENCY NAME(S) AND ADDRESS(ES)	10. SPONSOR/MONITOR'S ACRONYM(S)
	11. SPONSOR/MONITOR'S REPORT NUMBER(S)

12. DISTRIBUTION/AVAILABILITY STATEMENT
Approved for public release; distribution unlimited

13. SUPPLEMENTARY NOTES

14. ABSTRACT
Assessment of thruster induced contamination of critical surfaces is the important and necessary stage of International Space Station (ISS) component design. Plume contamination models aimed at the prediction of the spatial distribution of contaminant mass uxes have been developed in the recent years for various ISS thrusters based on vacuum chamber and space ight experiments and empirical correlations [1, 2]. Relatively scarce space ight contamination data have been gathered to date and are mostly limited to the measurements of thruster plume centerline contaminant uxes. It is necessary, however, to have detailed knowledge of the contaminant deposition as a function of the angle from the plume centerline especially, in the plume back ow region. The realization of this fact has motivated new ight experiments which are being planned for a future Space Shuttle mission

15. SUBJECT TERMS

16. SECURITY CLASSIFICATION OF:			17. LIMITATION OF ABSTRACT	18. NUMBER OF PAGES	19a. NAME OF RESPONSIBLE PERSON
a. REPORT **unclassified**	b. ABSTRACT **unclassified**	c. THIS PAGE **unclassified**		**11**	

experiments and plume models. An overlay Lagrangian particle tracking was used to track both particles in the plume core flow and those emanated from the cooling film, over a gas solution obtained using a Navier-Stokes equations and a DSMC solvers.

2 Thruster Conditions and General Numerical Methodology

The flow conditions and geometry considered in this work correspond to the bipropellant NTO/UDMH 130 N thruster. A conical nozzle geometry is used in this work with the following parameters. Throat diameter is assumed to be 1.55 cm, the exit-to-throat area ratio is 31.7, and the expansion angle of the diverging section is 20 deg. The propellant is UDMH/NTO, and the stagnation temperature and pressure are 2,900 K and 3.85 atm, respectively. Ten species mixture was used to model UDMH/NTO combustion products. The equilibrium combustion products composition for assumed oxidizer-to-fuel ratio of 2.0 as well as the calculated mixture composition at the nozzle exit are given in Table 1.

Table 1: Species mole fractions

Species	CO	CO2	H	H2	H2O	NO	N2	O	OH	O2
Chamber	0.183	0.042	0.053	0.146	0.259	0.005	0.257	0.008	0.037	0.005
Exit	0.235	0.120	0.004	0.012	0.255	0.008	0.354	0.002	0.002	0.008

The following three-step approach has been applied to model gas and particulate properties inside the nozzle and in the plume near field including the backflow region.

1. Gas-phase flow field solution in the thruster is obtained using Navier-Stokes solver;

2. Gas-phase flow field for the thruster plume expansion into vacuum is obtained using direct simulation Monte Carlo method;

3. Droplet velocities and number flux distributions inside the thruster and in the vacuum expansion region are calculated using particle tracing technique.

The following section gives a more detailed explanation of the numerical methodology.

3 Computational Approach

3.1 Gas Flow Inside the Nozzle

The numerical procedure starts with modeling of gas flow inside the nozzle. Since the density in that region is rather high, the continuum approach may reliably be used there.

The solution for the gas flowfield inside the nozzle (throat to exit) was obtained using VIPER (Viscous Interaction Performance Evaluation Routine) code, a two-phase two-dimensional reacting parabolized Navier-Stokes flow solver[10]. A structured rectangular grid with 520 cells in the axial direction and 100 cells in the radial direction (refined closer to the surface) was used.

3.2   Gas Flow in the Plume Near Field

The plume near field is characterized by significant gas rarefaction and strong gradients, especially in the nozzle lip region. To compute the plume this region, the continuum solution from the first step was used to generate a starting surface utilized as the inflow boundary condition for a DSMC-based code SMILE [11]. The starting surface was chosen to be a plane located at about X=0.8 L, where L is the length of the diverging section of the nozzle.

The important features of SMILE that are relevant to this work are parallel capability, different collision and macroparameter grids with manual and automatic adaptations, and spatial weighting for Axisymmetric flows. The majorant frequency scheme was used to calculate intermolecular interactions. The intermolecular potential was assumed to be a variable hard sphere. Energy redistribution between the rotational and translational modes was performed in accordance with the Larsen-Borgnakke model. A temperature-dependent rotational relaxation number was used. The reflection of molecules on the surface was assumed to be diffuse with complete energy and momentum accommodation.

3.3   Droplet Tracking Technique

Propellant droplets do not impact the gas flow due to their negligible concentration. A one-way coupling of liquid droplet and gas transport has therefore been used, that implies that particle trajectories will be calculated using pre-computed gas flow solution (obtained at steps one and two, see above).

Droplet tracking through the thruster and plume flowfield was employed to determine the droplet distribution and velocities for different droplet sizes. Droplet equation of motion through the gas flowfield was solved using the following approximation of the drag coefficient accounting for rarefaction and compressibility effects[9]:

$$c_D = 2 + (C_{D,0} - 2)\exp(-3.07\sqrt{(\gamma)}g(Re)M/Re) + \frac{h(M)}{\sqrt{(\gamma)}M}\exp(-\frac{Re}{2M}) \qquad (1)$$

where γ - is the ratio of the specific heats of the carrier gas, $Re = \dfrac{\rho_g U_{rel} d}{\mu_g}$ - Reynolds number, M - Mach number, ρ_g, μ_g - carrier gas density and viscosity, d - droplet diameter, and g and h are the two functions:

$$g(Re) = \frac{1 + Re(12.278 + 0/548Re)}{1 + 11.278Re}$$

$$h(M) = \frac{5.6}{1 + M}$$

and where $C_{D,0}$ is the drag coefficient for a $M = 0$ (standard curve). This expression for the drag coefficient is valid in a wide range of Mach and Reynolds numbers and ensures that C_D approaches the free molecular value for high Knudsen numbers.

4   Results and Discussion

4.1   General Flow Structure and Gas Backflow Contamination

It is known from on-the-ground and space experiments[12] that the surface contaminant of the 130 N UDMH/NTO thruster consists of two major groups, inorganic and organic materials. The inorganic part includes such surface degrading species as nitric acids, as well as species that may lead to their formation, such as nitric oxide and water. The organic part primarily includes amines, hydrazines, heterocycles, etc. For the considered type of thruster, a typical contaminant sample contains about 45% organic and 55% inorganic molecules. This composition results from complex processes that occur in a thin liquid layer. This layer forms due to spacecraft contamination from both gas (molecules and molecular clusters) condensate and liquid (propellant droplets) sources. Whereas the second source is conventionally regarded as the main one (its contribution is estimated at 90% in Ref. [12]), the molecular contamination may also be an important factor that affects the total contamination process. In order to better understand the molecular contamination, contributions from different molecular sources have to be assessed.

Let us first examine the general structure of the gas flow expanding through a conical nozzle, obtained using a combined continuum/kinetic approach. The overall gas velocity field is given in Fig. 2, where the solution obtained by the two methods is presented. The starting surface is shown by the dashed line located at X=0.085 m. Note that the actual continuum solution was obtained up to the nozzle exit. The starting surface was placed inside the nozzle in order to better resolve the flow near the nozzle lip. The transition from the continuum to the kinetic solution is smooth even in the subsonic part of the flow close to the surface, with the boundary layer thickness gradually increasing toward the exit. The streamlines in this figure also illustrate the continuum-to-kinetic handover. Note that the streamlines in the backflow region originate in a small region near the nozzle lip. This does not mean however that all molecules in the backflow come from the boundary layer. As was indicated in [7], most of the molecules in that region scatter back from the plume, not from the boundary layer. The backflow mass flow rate normalized to the total mass flow rate through the nozzle is equal to $\dot{m}_{bf}/\dot{m} = 7.503 \times 10^{-4}$.

The total gas number density field computed with the continuum and kinetic methods is given in Fig. 1. The conical contour of the diverging section results in a formation of a compression layer at the surface in the middle of the section, that detaches from the surface further downstream. The compression layer does not significantly impact the flow in the expansion region. As expected, the gas density (and mass flux) in the back flow is

many orders of magnitude smaller than at the exit. In order to analyze possible molecular contamination, though, it is essential to examine the contribution of different species into the total mass flux.

Figure 4 shows the distribution of mole fractions of different species normalized by the corresponding values at the nozzle axis at the exit plane (see Table 1). These distributions were taken along an arc with the center at the nozzle lip and the radius equal to the nozzle exit radius, $r_e = 4.375$ cm. The angle is counted anti-clockwise; the angle of 0 deg corresponds to the plume direction. It is clearly seen that there is a significant species separation even between water and nitric oxide. Water molecule mole fraction increase significantly in the backflow region because of its lower mass, and amounts to about a half of the total gaseous mass flow. Nitric oxide mole fraction drops in the backflow region compared to its plume core flow values. The decrease of the UDMH molecule mole fraction is even more significant, with minimum ratios at large angles as low as 0.2.

The most important contamination-related parameter is the mass flux of various contaminant species at different locations (or angles) in the plume and backflow. Figure 5 compares the total and some species mass fluxes along the arc mentioned above. Only larger angles are shown here to provide more details in the backflow region. The relative contribution of light molecules, such as water, increase, while that of heavier species decreases. Let us now compare the total molecular flux with the estimate given in [12]. In that paper, the amount of initial contaminant deposition from a 130 N thruster at angles of 100 to 110 deg and distances of about a radius from the nozzle lip was estimated at about 16 kg/m^2, based on experiments performed on Mir space station. Taking the average pulse duration of 50 ms and the total number of pulses of about 150,000 from [12], we have the average contaminant mass flux of 0.00213 kg/(m^{2}s). Interesting to note that this number coincides with the total molecular mass flux computed in this work (see Fig. 5).

4.2 Central Plume Droplet Contamination

Liquid drops of unburned propellant are present in the central plume region of small bipropellant thrusters due to the removal of the liquid phase directly from the combustion chamber[12] and shedding from the liquid film at the nozzle throat and their subsequent transport by the gas flow.[7] To model the transport of the droplets in the central plume region the droplets were traced starting at the nozzle throat through the gas flowfield inside the nozzle and in the plume region. The range of droplet radii considered was from 0.1 μm to 50 μm. The droplet initial velocities for different droplet sizes at the throat was calculated using a 1-D tracking over a gas flow solution based on ideal nozzle theory.

The calculated distribution of the X-component of velocity are shown in Fig. 6 for droplet radii of 1 μm (top) and 10 μm (bottom). It is seen that the for larger droplet sizes there is a significant velocity lag between the liquid droplets and gas stream and it has to be accounted for by compressibility corrections in the interphase momentum transfer model. A model of the droplet velocities in the plume of ISS thrusters was proposed in Ref. [1] based on droplet tracking for several other ISS thrusters. The comparison of the model from Ref. [1] to the

current calculations (see Fig. 7) shows that the model indeed gives a conservative estimate of the velocities for a wide range of the droplet sizes.

As it is seen from Fig. 6 the droplet spatial distribution in the central region is limited to a relatively narrow range of angles from the plume centerline. The calculated limiting angles are plotted in Fig. 8 for different droplet diameters. The limiting angle decreases nearly exponentially for increasing droplet sizes and is less than 13^0 for larger droplets. Experimental measurements of contaminant deposit density as a function of the angle from the plume centerline for this 130 N thruster were conducted in Keldysh Research Center[12]. The measured contaminant density decreased by more than an order of magnitude from the plume axis to the angle of about 30 deg. The contaminant deposit density was significant and decreased much more slowly (only about a factor of two) for angles from 30 to 90 deg. The current calculation of the transport of droplets originating in the chamber or at the nozzle throat shows that even droplets with radius smaller than 1 μm can not be found at angles more than 30 deg from the plume axis. This suggests that the droplets found experimentally at large angles must be introduced into the gas stream at a different location such as the nozzle lip region.

4.3 Peripheral Plume Droplet Contamination

The droplet contamination in the peripheral plume region for UDMH/NTO thrusters is connected to the effusion of liquid droplets from the film of unburned propellant near the nozzle exit lip.[12] Numerical computations of the transport of droplets emerging near and outside of the nozzle lip were first carried out by Ivanov *et al.*[7] The results of the computations confirmed the possibility of droplets to penetrate deep into the backflow. Here we calculate the transport of droplets emanating from the nozzle lip for 130 N thruster and compare the results for different initial conditions of the liquid film at the wall.

We consider three cases different in the position and speed of the droplets emanating from the nozzle lip. In all three cases the droplets of 100 μm are uniformly distributed over a starting surface near the nozzle lip with the initial velocity vector normal to the surface. Case 1 refers to the surface obtained by rotation about the plume axis of an arc confined between angles of -45 deg to 135 deg from the plume axis and the radius of 0.5 mm, with the center located 0.5 mm downstream from the lip. The initial speed of droplets was 0.5 m/s. Case 2 refers to the same initial speed of droplets and the same starting surface but the range of angles from 0 to 360 deg (full torus). Case 3 refers to the same geometry of the surface as in Case 2 but a smaller speed of 0.1 m/s.

For Case 1 the resulting droplet trajectories are plotted in Fig. 9. The droplet trajectories for other cases are qualitatively similar. In all three cases a significant fraction of the droplets are carried by gas into the backflow region. The droplet fraction versus the angle from the plume axis for the three cases is shown in Fig. 10. The largest fraction of droplets is observed at about 45 deg from the plume axis, which corresponds to the direction of gas streamlines in this region. Note also the second maximum of the droplet fraction at large angles which is related to the geometric location of the starting surface with respect to the gas streamlines.

These computations show that from 18.% (Case 1) to 28 % (Case 2) of the total number of droplets emanating from the film will contribute to the backflow region contamination (angles > 90 deg).

5   Conclusions

The molecular and liquid droplet thruster-induced contamination is studied numerically for a 130 N ISS bipropellant thruster using Navier-Stokes and DSMC gas flow solvers and a Lagrangian particle tracking. The molecular sources contributing to the inorganic components of the plume contaminant are estimated, and a qualitative characterization of the liquid droplet contribution to the organic part of contaminant is conducted.

Large species separation is observed in backflow region of the thruster plume, resulting in large mole fraction of water molecules in this region. The mole fraction of fuel (UDMH) molecules or other organic molecules present in the plume in trace concentrations decreases rapidly in the backflow region. The total calculated mass flux of the molecular contaminant in the backflow region compares very well with the experimental measurement on-board of Mir space station.

The liquid droplet transport in the central part of the plume is calculated using particle tracking. The droplet velocity in the plume central region agrees for various droplet radii with a conservative estimate of the previously developed velocity model for other ISS bipropellant thrusters. The spatial distribution of the droplets is confined to a narrow range of angles from the plume centerline. Therefore, large values of the off-centerline liquid droplet density observed experimentally must be attributed to sources of droplets other than combustion chamber and thruster interior region.

In the peripheral plume region, the trajectories and mass flux angular distribution of droplets emanated from the vicinity of the nozzle lip are computed. These droplets are formed as result of a break up of a film of unburned propellant on the thruster wall. The computations show that approximately 20 to 30% of all liquid film droplets will contribute to the organic part of the backflow contaminant.

References

[1] Larin, M., Lumpkin, F., and Stuart, P., Modeling Unburned Propellant Droplet Distribution and Velocities in Plumes of Small Bipropellant Thrusters, *AIAA Paper 2001-2816*, June 2001.

[2] C. Soares, R. Mikatarian, H. Barsamian, S. Rauer, "International Space Station Bipropellant Plume Contamination Model", AIAA Paper 2002-3016.

[3] F. E. Lumpkin III, K. C. Albyn, T. L. Farrell, "The Plume Impingement Contamination II Experiment: Motivation, Design and Implementation Plan", AIAA Paper 2001-2815.

[4] N.A. Gatsonis, R. Nanson, G.J. Lebeau, "Navier-Stokes/DSMC Simulation of Cold-Gas Nozzle/Plume Flows and Flight Data Comparisons", AIAA Paper 99-3456.

[5] I.D. Boyd, K.C.Kannenberg, K.K. Kossi, D.A.Levin, and D.P.Weaver, " Modeling the Plume Contamination and Emissions of an Ammonia Arcjet", AIAA 98-3505.

[6] D. J. Kirshman, "Contamination Environment Resulting from IUS Stage II Motor Post-burn Outgassing", Proceeding of International Symposium on Optical Science and Technology SPIE's 47th Annual Meeting, July 7-11, 2002, Seatle, WA.

[7] Ivanov, M.S., Khotyanovsky, D.V., Kudryavtsev, A.N., Vashchenkov, P.V., Markelov, G.N., Schmidt, A.A. "Numerical study of backflow for nozzle plumes expanding into vacuum," AIAA Paper 2004-2687.

[8] C. Soares, H. Barsamian, S. Rauer, "Thruster Plume Induced Contamination Measurements from the PIC and SPIFEX Flight Experiments", Proceedings of International Symposium on Optical Science and Technology SPIE's 47th Annual Meeting, July 7-11, 2002, Seatle, WA.

[9] Crowe, C., Sommerfeld, M., and Tsuji, Y., *Multiphase Flows with Droplet and Particles*. CRC Press, 1998.

[10] Kawasaki, A., Coats, D., and Berker, D., "A Two-Phase, Two-dimensional, Reacting Parabolized Navier-Stokes Flow Solver for the Prediction of Solid Rocket Motor Flow-fields", *AIAA Paper 92-3600*, 1992.

[11] Ivanov, M.S., Markelov, G.N., Gimelshein, S.F., "Statistical simulation of reactive rarefied flows: numerical approach and applications", *AIAA Paper 98-2669,* June 1998.

[12] Rebrov, S. and Gerasimov, Y., "Investigation of the Contamination Properties of Bipropellant Thrusters", *AIAA Paper 2001-2818*, June 2001.
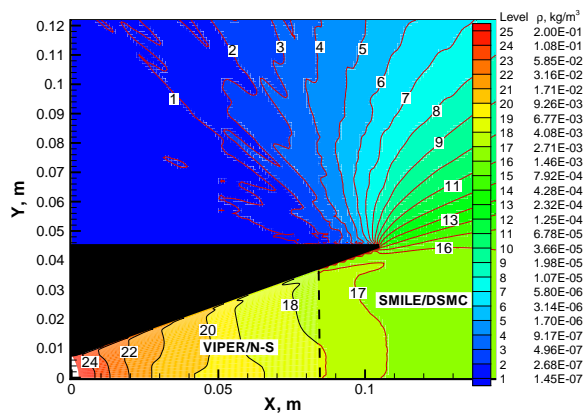
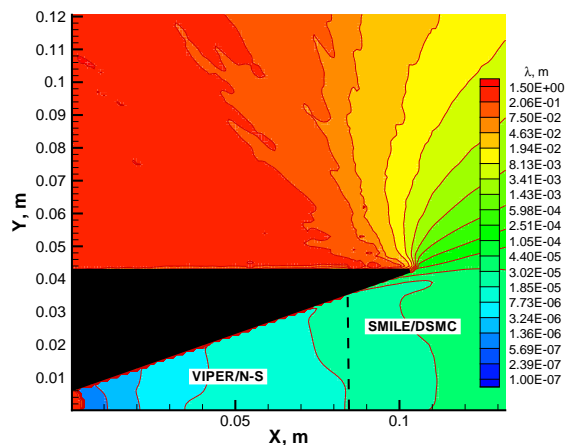Figure 1: Gas density (kg/m^3) flow field.

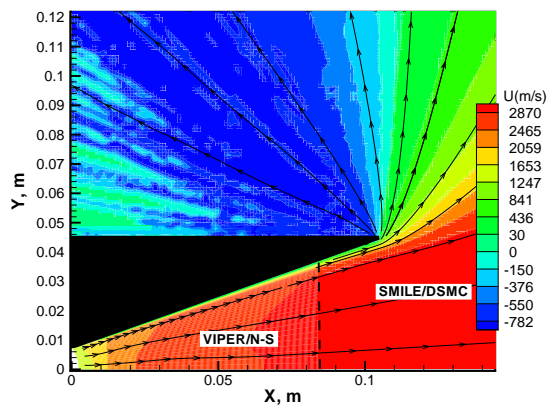

Figure 3: Gas mean free path (m) flow field.

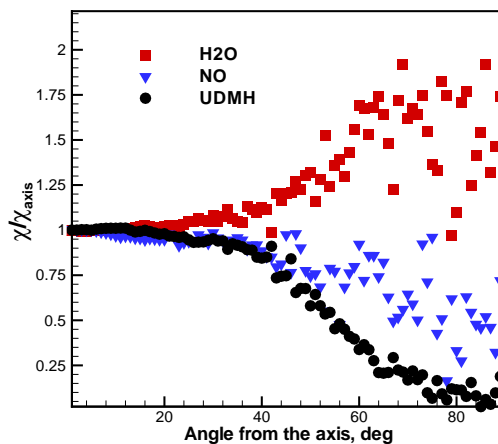Figure 2: Gas X-component of velocity (m/s) flowfield and gas streamlines.

Figure 4: Species fractions in the backflow normalized by the value at the plume axis.
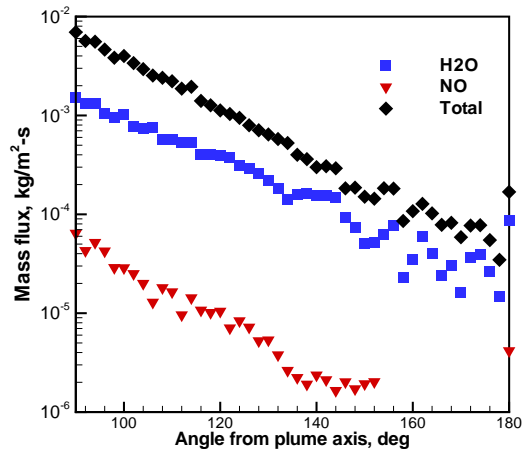
Approved for public release; distribution unlimited

Figure 5: Mass flux (kg/m$^2\cdot$ s) *vs* angle at the distance of 1 exit radius from the nozzle lip.
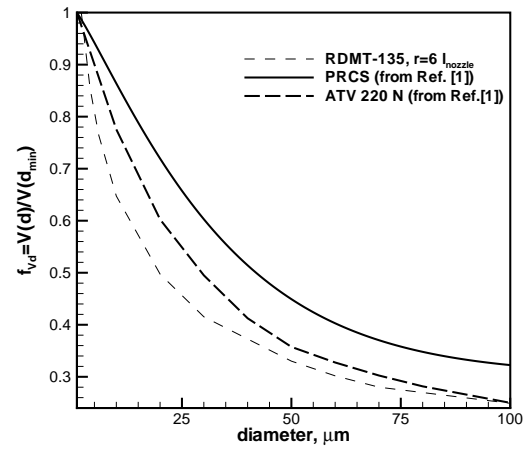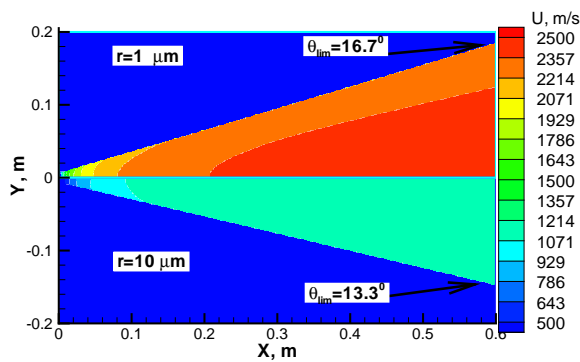

Figure 7: Droplet velocity (m/s) *vs* droplet diameter(micron).

Figure 6: X-component of velocity (m/s) distribution in the plume for droplets with radius of 1 μm and 10 μm.
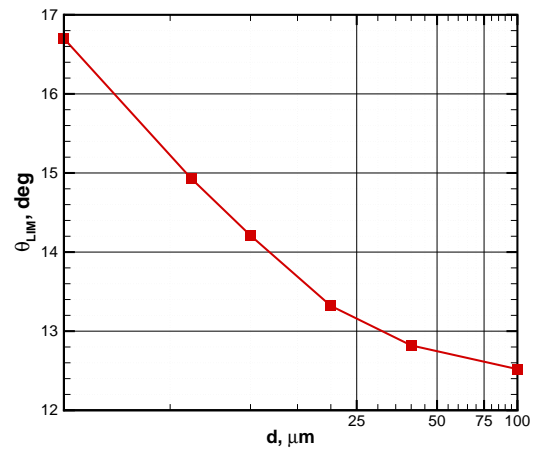

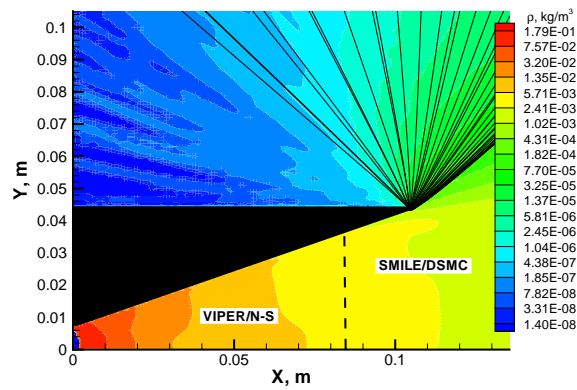Figure 8: Limiting angle (deg) *vs* droplet diameter(micron).
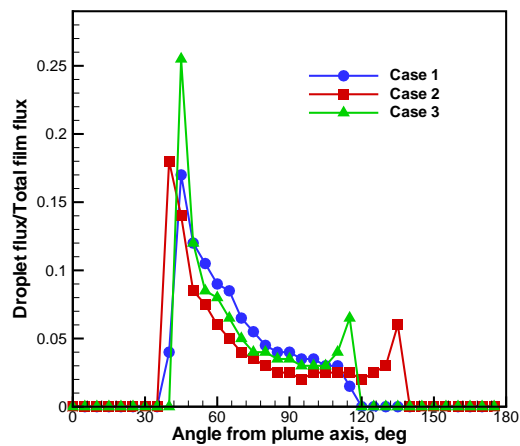
Figure 9: Trajectories of droplets emanating from the nozzle lip for Case 2.

Figure 10: Droplet fraction *vs* angle.